Experimental Investigation of a Layered Graphite/BN Channel for Hall Thrusters

IEPC-2011-192

Presented at the 32^{nd} *International Electric Propulsion Conference,*
Wiesbaden, Germany
September 11–15, 2011

Serge Barral*
Institute of Plasma Physics and Laser Microfusion, 01-497 Warsaw, Poland

Stéphan Zurbach†
Snecma, Safran Group, 27208 Vernon, France

and

Michel Dudeck‡
Université Pierre et Marie Curie - Paris 6, 75252 Paris Cedex, France

With a view to reduce leakage currents through graphite walls, two Hall thruster channels made of graphite layers isolated by thin ceramic coatings have been tested over a wide range of operating parameters. Measurements show that, beyond a discharge voltage threshold of the order of $400 - 500\,\mathrm{V}$, the thruster operates in a very quiet and efficient mode, in contrast to the low-efficiency space charge saturation regime observed with dielectric ceramic walls at high voltage.

I. Introduction

The low sputtering rate of carbon under heavy ion bombardment (Fig. 1) make it an interesting plasma-facing material in various ion sources. The replacement of molybdenum by carbon-carbon or pyrolitic graphite has been for this reason under investigation for many years in ion thruster optics, where it promises large enhancements in thruster lifetime. Likewise, the replacement of conventional BN-based ceramics by carbon-based materials is expected to bring significant benefits to Hall thrusters in terms of lifetime,[1–4] and may theoretically even improve efficiency owing to the low secondary electron emission (SEE) of carbon-carbon and graphite (Fig. 2). In Hall thrusters, however, the electrical conductivity of graphite has non-trivial side effects that may result in a large part of the discharge current flowing within the channel walls, thereby short-circuiting the plasma column. Arcing is another potential issue related to the conductivity of graphite, and was found critical in the case of carbon velvet segments.[3] Although empirical evidence suggests that plasma short-circuiting is not critical for short graphite segments,[1,4] a sizable impact on the efficiency has been measured[2] and theoretically predicted[5] for long segments which extent is comparable to that of the region subject to sputtering.

The use of diamond walls has been proposed to circumvent in-wall conductivity while retaining the advantages of carbon-based materials in terms of resistance to sputtering.[13] The scope of past experiments[14] remains too limited, however, to assess whether manufacturing issues can be fully addressed and whether the typically high SEE of diamond is a concern. Another relatively straightforward solution to the problem of conductivity would consist in the use of a homogeneous graphite-insulator composite, but the percolation

*Assistant Professor, Division of Magnetized Plasmas, sbarral@ipplm.pl.
†R & D Engineer, Space Engines Division, stephan.zurbach@snecma.fr.
‡Professor, Institut Jean le Rond d'Alembert, dudeck@ida.upmc.fr.

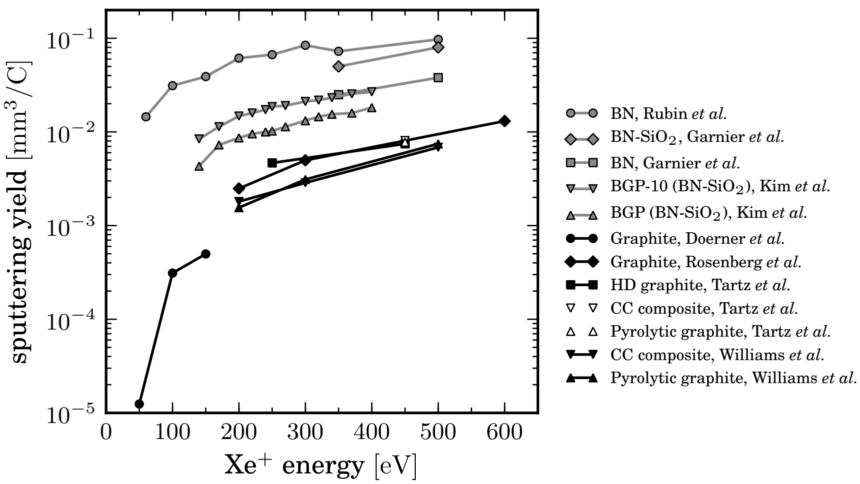

Figure 1: Sputtering yields of BN-based and carbon-based materials under Xe$^+$ bombardment at normal incidence and at room temperature.[6–12] A density $\rho = 2.2 \times 10^3\,\mathrm{kg/m^3}$ for BGP and BGP-10 has been assumed to convert data from V. Kim *et al.*[8] A density $\rho = 2.0 \times 10^3\,\mathrm{kg/m^3}$ for carbon-based materials has been assumed to convert all carbon-related data.[9–12]

threshold for conductivity is usually very low with a graphite phase and does not allow the graphite volume fraction to exceed $10 - 15\%$.[15] In this paper, a third solution is suggested and investigated whereas electrically conducting layers of graphite are separated by thin insulating layers. In analogy to the reduction of eddy currents in laminated core transformers, the proposed layered composite is expected to significantly reduce plasma short-circuiting through the walls. Material properties other than electrical conductivity (in particular, sputtering and SEE) should remain, however, similar to that of a homogeneous graphite segment from the perspective of plasma-wall interactions.

It is important to underline that the two experiments reported here (z-partitioning and z, θ-partitioning of the channel) have been conducted more than three years apart and that the SPT-100ML used in both experiments has experienced some modifications between these experimental campaigns (anode and cathode changes, among others). We have therefore chosen to report the results of these two experiments in dedicated sections and have refrained from quantitative comparisons between them.

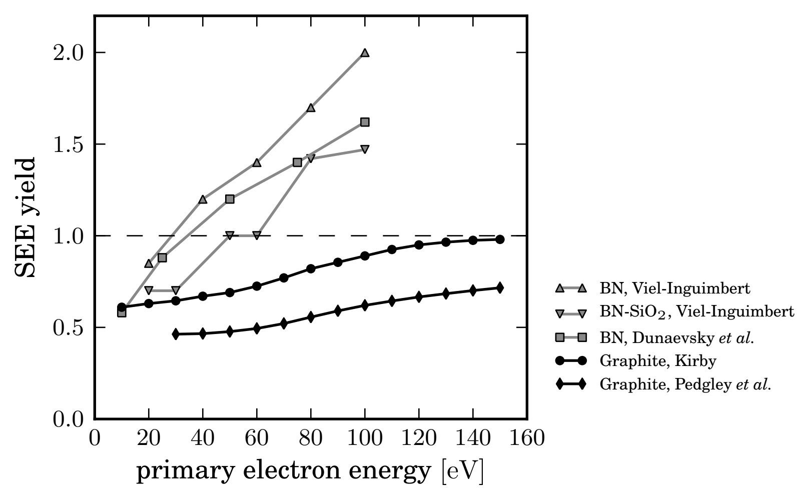

Figure 2: Secondary electron emission yields of BN-based and carbon-based materials electron bombardment at normal incidence and at room temperature.[16–19]

II. Theoretical background

A. Overview

It is interesting to note that the use of conducting walls in Hall thruster was initially mostly motivated by the desire to tailor the electric field profile and control the topology of the ionization and acceleration zones.[20–23] Following the limited success of such strategy, however, later studies have instead focused on channel lifetime and have for this reason used carbon-based segments placed near the channel exit.[1–4] The present study intends to go further by actually preventing electrical conduction within sputter-resistant segments, using a layered graphite/insulator composite meant to retain the advantages of graphite in terms of sputtering and SEE, but acting similarly to an insulator at the macroscopic level. This idea, illustrated by Fig. 3, is easily understood, but the notion of what is indeed *macroscopic* remains of course meaningless unless a characteristic scale is defined.

The relatively simple criterion from which we shall derive such characteristic scale can be expressed as follows:

> *the thickness of a conducting layer shall be such that the additional electron conductivity provided by in-wall currents be less than or equal to classical near-wall conductivity.*

We shall later refer to such material as a *pseudo-insulator.*

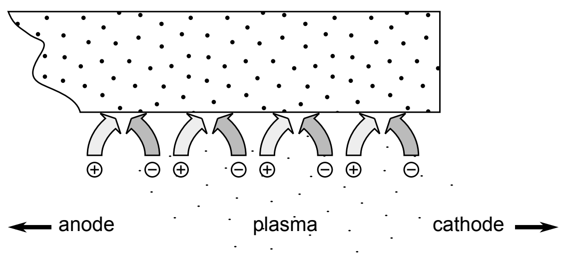

(a) insulating wall

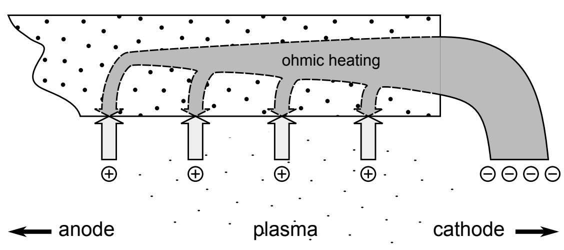

(b) conducting wall

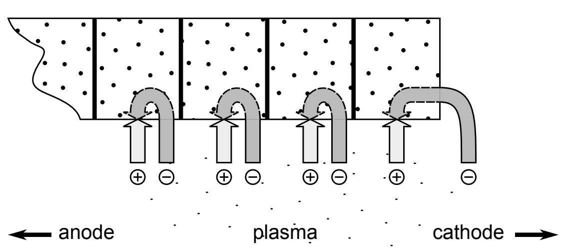

(c) partitioned conducting wall with insulating interfaces

Figure 3: Schematic representation of ion and electron currents with insulating, conducting and partitioned conducting walls.

B. Main assumptions

We suppose that the thickness a of every partition is small in comparison with the typical scale on which the plasma parameters change, so that for each elementary partition the relationships,

$$T_e = \text{const} \tag{1}$$
$$E_z = \text{const} \tag{2}$$

hold over the whole plasma-sheath interface, where T_e is the electron temperature and E_z the axial electric field.
Assuming moreover that the bulk material is a perfect electrical conductor, the potential within the element is considered uniform, *i.e.*

$$\Phi_w = \text{const}\,. \tag{3}$$

C. Critical thickness for axial partitioning

The critical thickness shall be estimated based on the above stated criterion, *i.e.* such that the shunt current within a partition be less than the near-wall current pertaining to this same partition.

In order to estimate the shunt current I_{sh} (*i.e.* the axial component of the current within a graphite partition), we consider a partition located between $z = z_0$ and $z = z_0 + a$. By virtue of equation (2), the axial variation of plasma potential at the sheath edge in front of the partition is of the form

$$\Phi(z) = \Phi_0 - E_z\, z, \tag{4}$$

which gives in turn the expression for the variation of the sheath potential:

$$\Phi_s(z) = \Phi_0 - \Phi_w - E_z\, z\,. \tag{5}$$

The shunt current within the wall partition at position z is given by

$$I_{sh}(z) = e \int_{z_0}^{z} \left[\Gamma_{iw}^{-} - \Gamma_{ew}^{-}\,(1-\bar{\sigma})\right] dz\,, \tag{6}$$

where $\bar{\sigma}$ is the effective SEE yield and Γ_{iw}^{-}, Γ_{ew}^{-} are the ion and electron linear flux densities towards the walls, respectively. Since the partition is electrically insulated at both ends, I_{sh} satisfies the additional boundary condition:

$$I_{sh}(z_0 + a) = 0\,. \tag{7}$$

The flux densities of ions and electrons toward the walls per unit of axial length are as usual given by

$$\Gamma_{iw}^{-} = 2\pi\,(R_1 + R_2)\; n_e \sqrt{\frac{\kappa T_e}{m_i}}\,, \tag{8}$$
$$\Gamma_{ew}^{-} = 2\pi\,(R_1 + R_2)\; n_e \sqrt{\frac{\kappa T_e}{2\pi m_e}} \exp\left(-\frac{e\,\Phi_s}{\kappa T_e}\right), \tag{9}$$

where n_e must be understood as the density at the sheath edge and $\sqrt{\frac{\kappa T_e}{m_i}}$ stands for the Bohm velocity.
In the light of equation (1), it can be deduced that Γ_{iw}^{-} is approximately constant for a given partition. Let us also mention that the space charge limitation on Γ_{ew}^{-} does not apply here since the effective SEE yield of graphite should not exceed the charge saturation value (≈ 0.98 for xenon).

The effect of I_{sh} on the *global* conductivity is in turn given by its average value along z. This will become more obvious if one contemplates the expression of the axial potential drop in the plasma as a function of the total current:

$$\Phi(z_0 + a) - \Phi(z_0) = \int_{z_0}^{z_0+a} \left[\frac{1}{\mu_e}\left(\frac{I_d - I_{sh}}{n_e e A} - V_{iz}\right) - \frac{1}{e\,n_e}\frac{d\,(n_e \kappa T_e)}{dz}\right] dz\,. \tag{10}$$

where μ_e is the plasma conductivity and A the plasma column cross-section. Since a is considered small, the ratio $1/\mu_e n_e$ remains approximately constant between z_0 and $z_0 + a$ and the contribution of I_{sh} to the global conductivity can thus be estimated from the simple average

$$\begin{aligned}\overline{I}_{sh} &= \frac{1}{a}\int_{z_0}^{z_0+a} I_w(z^*)\,dz^* \\ &= e\int_{z_0}^{z+a} dz^* \int_{z_0}^{z^*} \left[\Gamma_{iw}^- - \Gamma_{ew}^-\left(1-\overline{\sigma}\right)\right] dz\,. \end{aligned} \tag{11}$$

Using equations (3, 5, 7, 8, 9), it is possible to transform without further approximations the former relationship into the more useful form

$$\overline{I}_{sh} = e\,\Gamma_{iw}^-\,a\left[\frac{1}{2} - \frac{\kappa T_e}{e\,E_z\,a} + \frac{1}{\exp\left(\dfrac{e\,E_z\,a}{\kappa T_e}\right)-1}\right]. \tag{12}$$

The behavior of $\overline{I}_{sh}$ as a function of a is quadratic for thin partitions:

$$\overline{I}_{sh} \overset{a\to 0}{\sim} e\,\Gamma_{iw}^-\,\frac{e\,E_z}{12\,\kappa T_e}\,a^2 \tag{13}$$

and linear for thick partitions:

$$\overline{I}_{sh} \overset{a\to\infty}{\sim} e\,\Gamma_{iw}^-\left(\frac{a}{2} - \frac{\kappa T_e}{e\,E_z}\right). \tag{14}$$

We shall now estimate the classical cross-field current due to electron scattering on the walls. For the sake of simplicity, we limit our analysis to the high magnetic field region of the channel where the influence of walls is the most critical. In this region, the axial wall-induced current can be estimated from the simple Ohm's law for cross-field transport:

$$I_{ez} = \frac{e^2}{m_e}\frac{\nu_{ew}}{\omega_{ce}^2}n_e E_z = \frac{e^2}{m_e}\frac{\Gamma_{ew}^-}{\omega_{ce}^2}E_z \tag{15}$$

and, since the plasma parameters change slowly over the axial extend of the partition, its average value in front of a partition can be defined as

$$\overline{I}_{ez} = \frac{e^2}{m_e}\frac{1}{\omega_{ce}^2}E_z\,\frac{1}{a}\int_{z_0}^{z_0+a}\Gamma_{ew}^-\,dz\,. \tag{16}$$

The balance of currents within a partition is given by equation (7) and states that

$$\int_{z_0}^{z_0+a}\left[\Gamma_{iw}^- - \Gamma_{ew}^-\left(1-\overline{\sigma}\right)\right]dz = 0. \tag{17}$$

Since the thermal energy of electrons impinging the walls is weakly dependent on the sheath potential[a], the SEE yield can be treated as a constant in the former relationship. Besides, Γ_{iw}^- remains as mentioned earlier approximately constant for a given partition, so that equation (16) can be finally rewritten

$$\overline{I}_{ez} = \frac{e^2}{m_e}\frac{\Gamma_{iw}^-}{1-\overline{\sigma}}\frac{1}{\omega_{ce}^2}E_z, \tag{18}$$

or in the alternative form:

$$\overline{I}_{ez} = e\,\frac{\Gamma_{iw}^-}{1-\overline{\sigma}}\,r_{ce}, \tag{19}$$

where r_{ce} stands for the electron cyclotron radius.

[a] The thermal energy of electrons at the walls is actually rigorously independent from Φ_s for the particular case of a Maxwellian electron distribution.

We may now deduce the condition on the thickness a by applying the criterion for a *pseudo-insulator* stated earlier, *i.e.* by satisfying

$$\overline{I}_{sh} \leq \overline{I}_{ez} \,. \tag{20}$$

Using the assumption (to be justified later) of thick partitions, we use equation (14) to transform this condition into:

$$a \leq \frac{2 r_{ce}}{1-\overline{\sigma}} + \frac{2\kappa T_e}{e\, E_z} \,. \tag{21}$$

It is known, however, that the thermal energy in the high magnetic field region comes mainly from cyclotron rotation. Assuming additionally pressure isotropy, the temperature in the high magnetic field region can be approximated as

$$\kappa T_e \approx \frac{1}{3} m_e \left(\frac{E_z}{B_r}\right)^2 = \frac{1}{3} e\, E_z\, r_{ce}, \tag{22}$$

which lets us rewrite condition (21) as a simpler design requirement, either in the form:

$$a \leq \frac{\kappa T_e}{e E_z} \left(\frac{6}{1-\overline{\sigma}} + 2\right) \,, \tag{23}$$

or alternatively:

$$a \leq r_{ce} \left(\frac{2}{1-\overline{\sigma}} + \frac{2}{3}\right) \,. \tag{24}$$

Equation (23) provides a justification *a posteriori* for the thick partition hypothesis, as it shows that the critical value of a is of the order of $8\kappa T_e / e E_z$ or higher.

D. Interpretation of the critical thickness

Equation (24) shows that the critical partition thickness is proportional to the electron cyclotron radius. This can be understood from a phenomenological viewpoint if one remembers that the classical wall-induced current is due to the scattering of impinging electrons and/or to the subsequent emission of secondary electrons at the walls. In a strongly confining magnetic field, electrons (re-)emitted from the walls with a random phase will on the average be displaced by a an axial distance of the order of the cyclotron radius before they perform the next collision. However, in-wall conductivity allows electrons impacting a wall to travel *within* the wall before they are re-emitted. Since electrons tend to enter a wall partition where the plasma potential is the lowest and re-enter the plasma where its potential is the highest, they actually travel a distance that is typically of the order of the partition thickness. The additional conductivity provided by the shunt effect derives thus from the additional axial displacement of electrons flowing through the walls. Therefore, if the wall is to behave mostly as an insulator, one may expect that the partition thickness should be at most of the order of magnitude of the cyclotron radius.

E. Critical azimuthal angle for azimuthal partitioning

Shunt currents induced by azimuthal variations of the plasma potential may justify partitioning of the channel along the azimuth. Among the possible origins for azimuthal electric fields, one can mention:

- geometrical factors: misalignment between the channel axis and the axis of the magnetic poles, azimuthal variations of the magnetic strength inherent to the magnetic system (*e.g.* peripheral coils on SPT-type thrusters), influence of the cathode . . . ,
- plasma waves: spoke instability[24, 25] or other low frequency azimuthal instabilities.[26] Hopefully, high frequency instabilities are too fast to affect the wall sheath.

The theoretical analysis of section C can be straightforwardly transposed to the case of azimuthal currents by comparing the azimuthal shunt current to the component $I_{e\theta}$ of the wall-induced cross-field current[b].

[b] $I_{e\theta}$ is not meant here as a Hall current, but as the component of cross-field current which arises from the fact that $\mathbf{E}$ is tilted in the referential of the channel.

Proceeding as before and assuming that the azimuthal angle $\Delta\theta$ of each partition is small with respect to the azimuthal periodicity of the plasma parameters (E_θ, T_e, ...), the counterpart of equation (23) is obtained:

$$R\,\Delta\theta < \frac{\kappa T_e}{e\,|E_\theta|}\left(\frac{6}{1-\overline{\sigma}}+2\right) \tag{25}$$

where R is the channel wall radius or, if the counterpart of equation (24) is sought:

$$R\,\Delta\theta < \frac{E_z}{|E_\theta|} r_{ce}\left(\frac{2}{1-\overline{\sigma}}+\frac{2}{3}\right) \tag{26}$$

Extrapolating slightly these results, equation (23) and equation (25) can be synthesized with the condition

$$\sup(\Phi) - \inf(\Phi) < \frac{\kappa T_e}{e}\left(\frac{6}{1-\overline{\sigma}}+2\right) \tag{27}$$

which shows that the partition scheme actually aims at reducing the plasma potential variation in front of each partition.

III. Implementation

A. Materials and manufacturing

Two sets of composite segments have been made: one set with z-partitioning, constituted from stacked graphite rings, and one set with $z-\theta$ partitioning, constituted from an assembly of ring arcs. For both sets, the graphite elements priorly coated with a thin BN layer (except on plasma-facing surfaces) and maintained together with a mechanical assembly, as shown in Figs 4 and 5. Auxiliary mechanical components (supporting rings and fasteners) were made of alumina.

The BN layer was deposited on graphite using chemical vapor deposition (CVD). Due to the nature of the CVD process, coating thickness was not perfectly uniform; average thickness was of the order of 5/100 mm. Posterior to coating, the graphite elements have been laser-cut in order to expose the raw graphite on plasma-facing surfaces.

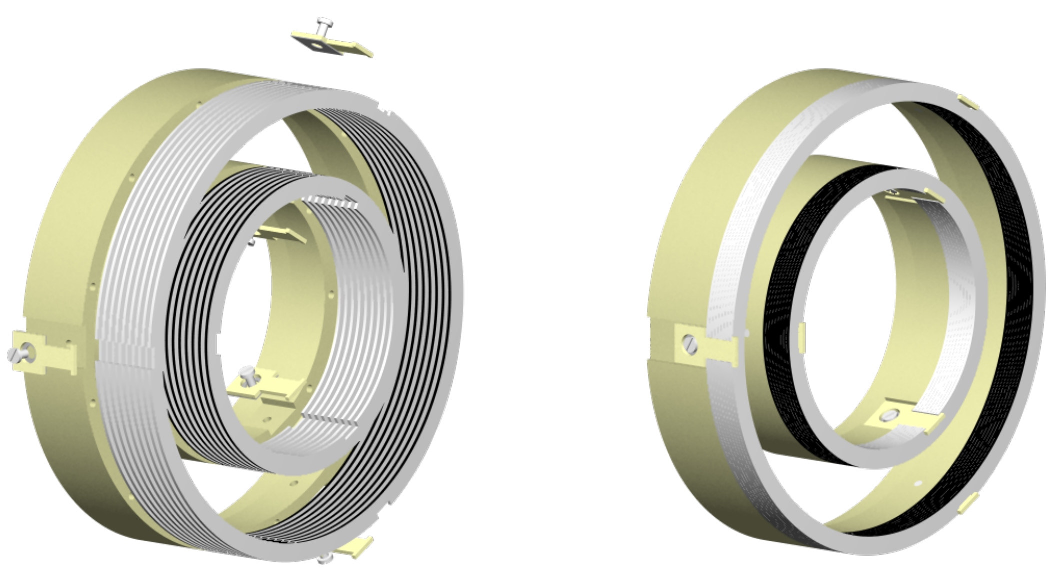

Figure 4: Schematic of the channel with axial (z) partitioning only.

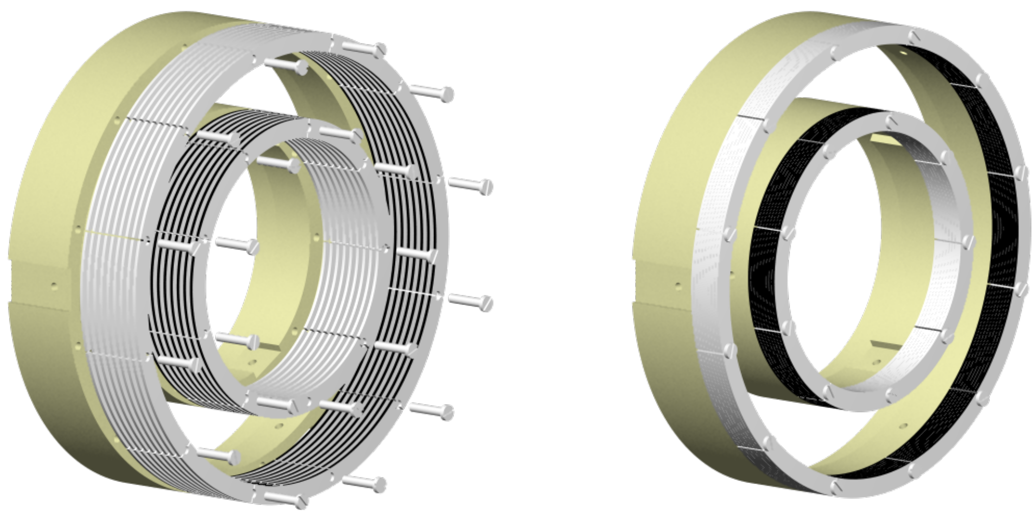

Figure 5: Schematic of the channel with both axial and azimuthal ($z - \theta$) partitioning.

B. Geometry

Taking a minimum nominal discharge voltage $U_d = 300\,\text{V}$, the potential drop inside the channel was assumed equal to $\Delta U = 200\,\text{V}$. Under such conditions, numerical simulations suggest[5] that the electron cyclotron radius varies between 0.4 mm and 0.5 mm over the last centimeter of the channel, and we take therefore

$$r_{ce} = 0.4\,\text{mm} .$$

Assuming an effective SEE yield $\overline{\sigma} = 0.5$ and using equation 24, the maximal partition thickness is:

$$a \leq 2.3\,\text{mm} .$$

For the sake of safety, a thickness $a = 0.8\,\text{mm}$ was ultimately taken.

It is obvious that theoretical predictions regarding the azimuthal partition scheme are much more speculative since the azimuthal electric field profile and variation is not known. Let us suppose that the azimuthal field is due to a misalignment between the magnetic system and the channel axes. Taking for instance a misalignment angle of $\alpha = 2°$ and remarking that the maximum of the azimuthal component of the electric field is $E_\theta = E_z \tan\alpha$, the maximum azimuthal extend of a partition is obtained:

$$R\Delta\theta < 65\,\text{mm} .$$

For a SPT-100 type thruster, this would mean that at least five elementary partitions are required along the azimuth on the outer ring, and four on the inner ring. Ultimately, 12 azimuthal partitions on the outer diameter and 9 azimuthal partitions on the inner diameter have been used.

The total height of the segments was about 10 mm in the case of z-partitioning, and about 9 mm in the case of z, θ-partitioning.

C. Experimental conditions

Both experimental sessions have taken place in Orléans (France) in the PIVOINE facility of the ICARE laboratory (CNRS), using the PPS-100ML laboratory Hall thruster. As mentioned in introduction, it is important to remember that experiments with z-partitioning and z, θ-partitioning have been conducted more than three years apart and that modifications of the thruster have occurred between these experiments, making quantitative comparisons between them difficult.

In both experiments, the cathode flow rate was maintained at 0.4 mg/s. The vessel pressure was kept within the range $2-3\times10^{-5}$ mbar in all cases. Unless otherwise indicated, the coils current was 4.5 A in all experiments.

IV. Results for axial (z) channel partitioning

It was rapidly observed that, efficiency-wise, optimal operation with the composite channel demands lower mass flow rates than with the baseline BN-SiO_2 channel. This is made obvious by Fig. 6, where efficiency is optimal at 4 mg/s (vs 5 mg/s for the nominal operating point with BN-SiO_2). Although at such moderate voltage (300 V) the efficiency with the composite channel would rarely match the efficiency of the baseline thruster, it was always much greater than the efficiency with homogeneous graphite segments, which appears to validate the premises of the pseudo-insulator design. Although it is difficult to compare directly with the study of Ref. 2 which predates those results by several years, it seems likely that the efficiency with the composite is greater than it would be with any non-BN ceramic.

At larger discharge voltages (Fig. 7), anode efficiency remained stable slightly below 50% up to a threshold around 500 V. Beyond this threshold, the operation of the thruster changed radically and was characterized by a very quiet low-frequency spectrum and a very high thrust efficiency. A sharp change in the fundamental breathing frequency is also observed, going from $10-15$ kHz up to $20-25$ kHz. Although it has proved impossible to operate the baseline (BN-SiO_2) thruster at such high voltage during this campaign, the high efficiency with the composite would certainly not be matched, especially considering the systematic appearance of the low-efficiency space charge saturation regime at high voltage with BN-SiO_2[2] which is actually already present at 500 V as shown by Fig. 7.

At the time of this first experimental campaign, the promising high-voltage behavior of the composite with z-partitioning could unfortunately not be investigated further due to time constraints and to the fear that the intense heating beyond 500 V could eventually melt brazed joints used on the alumina fasteners.

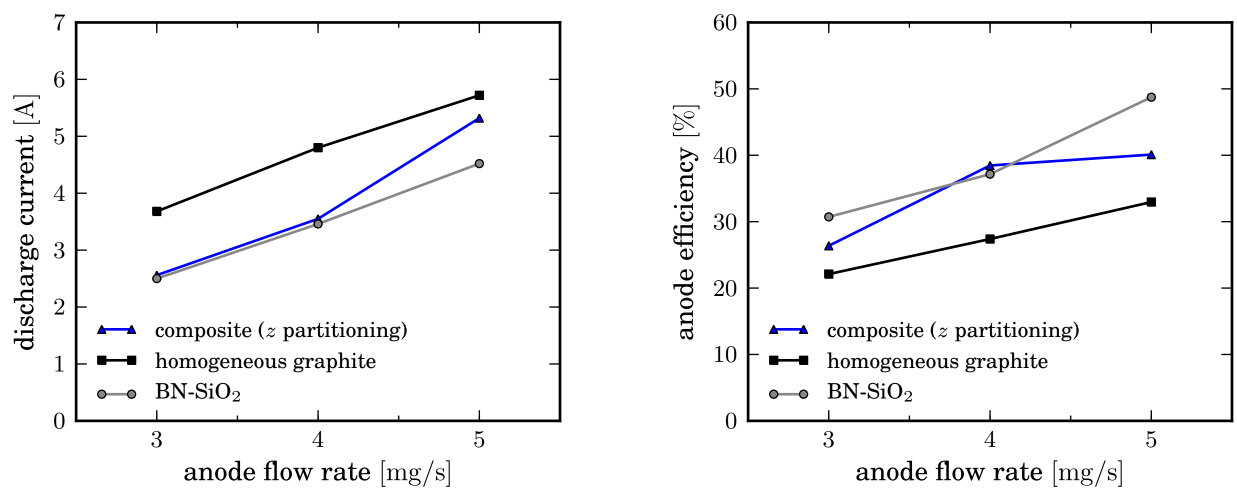

Figure 6: Average discharge current and anode efficiency as a function of the anode mass flow rate with z-partitioning and $U_d = 300$ V, compared to the baseline BN-SiO_2 channel and to a homogeneous graphite segment in the same conditions.

V. Results for axial-azimuthal (z,θ) channel partitioning

As in the case of z-partitioning, operation is more efficient for anode mass flow rates lower than the nominal mass flow rate of the baseline configuration. The influence of the discharge voltage has therefore been investigated at 3 mg/s and 4 mg/s (Figs 8 and 9).

At low and moderately high voltages, operation is characterized by a very narrow-spectrum breathing mode which takes the form of regular high current pulses as the voltage is increased, witnessed by the strong harmonic content of the signal. For both mass flow rates, a threshold voltage exists beyond which the thruster

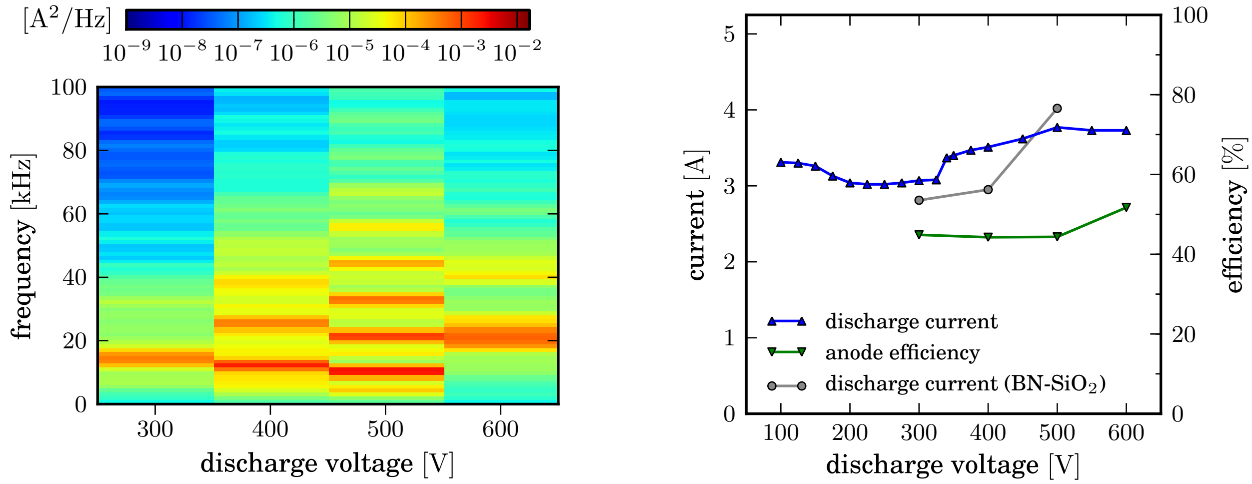

Figure 7: Power spectral density of the discharge current, average discharge current and anode efficiency as a function of the discharge voltage with z-partitioning and $\dot{m} = 3.5\,\mathrm{mg/s}$. The discharge current for the baseline BN-SiO$_2$ channel is provided for reference.

enters a very quiet, high efficiency operation mode. This high voltage mode is very similar to what has been previously observed with z-partitioning although the threshold voltage is lower with z, θ-partitioning, of the order of 400 V instead of 500 V. This correlation with the earlier experiment is very encouraging and, having in mind the long time interval between the experiments and the differences in configurations, appears to rule out the possibility that previous observations of this transition be accidental. Unlike the previous experiment, it has been possible to thoroughly investigate this high voltage mode during several consecutive hours of operation. Despite the rather large power at which the thruster was operated, no overheating of the graphite could be observed with the naked eye. In contrast, overheating of the alumina screw heads located in the exit plane was made obvious by the emission of a constant bright red-yellow light (Fig. 10), believed to be caused by the formation of a space charge saturated sheath and of a large local electron current due to the high SEE yield of alumina.

Further investigations at 500 V have shown that the transition to an efficient regime is more difficult at higher magnetic fields (Fig. 11), while an optimum in terms of anode mass flow rate seems to exist in the neighborhood of 3 mg/s (Fig. 12).

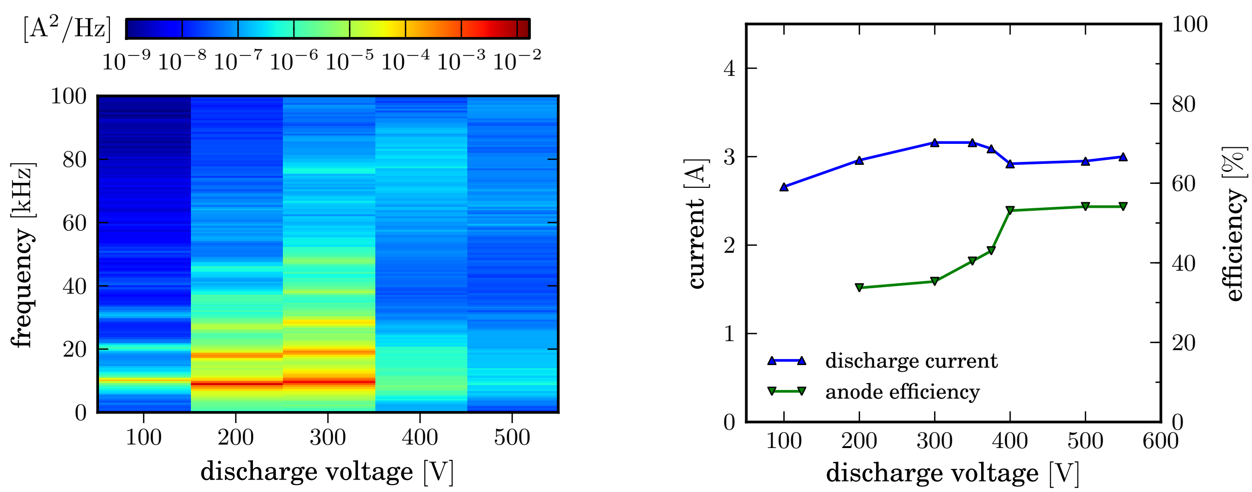

Figure 8: Power spectral density of the discharge current, average discharge current and anode efficiency as a function of the discharge voltage with z, θ-partitioning and $\dot{m} = 3\,\mathrm{mg/s}$.

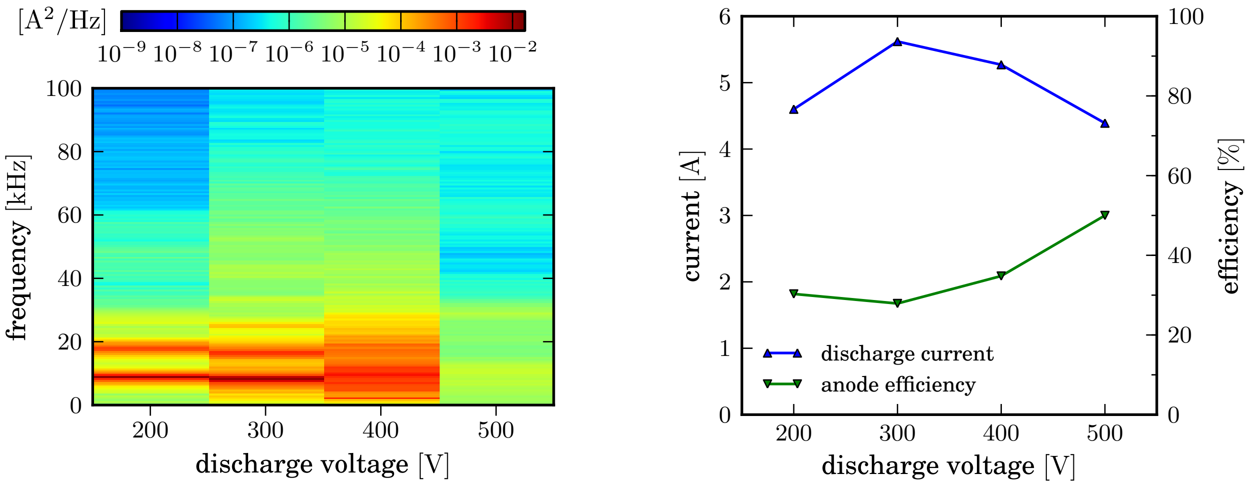

Figure 9: Power spectral density of the discharge current, average discharge current and anode efficiency as a function of the discharge voltage with z, θ-partitioning and $\dot{m} = 4\,\mathrm{mg/s}$.

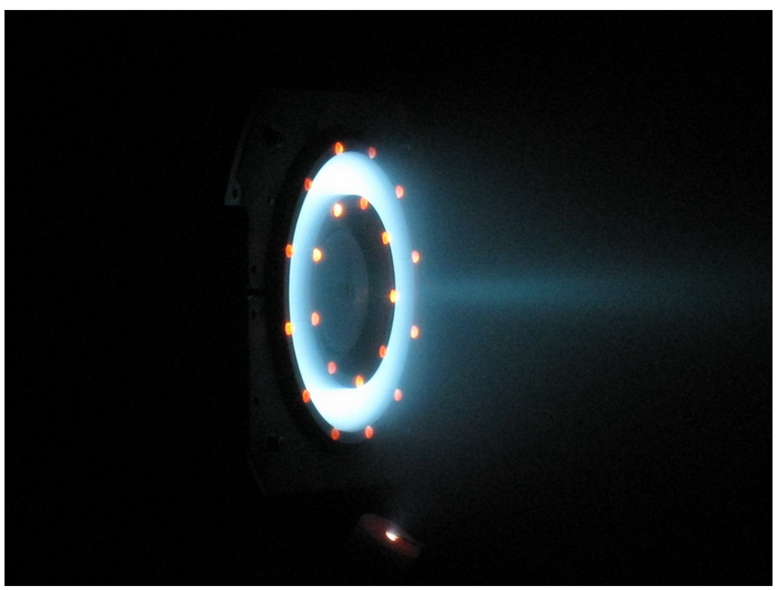

Figure 10: High power thruster operation with z, θ-partitioning.

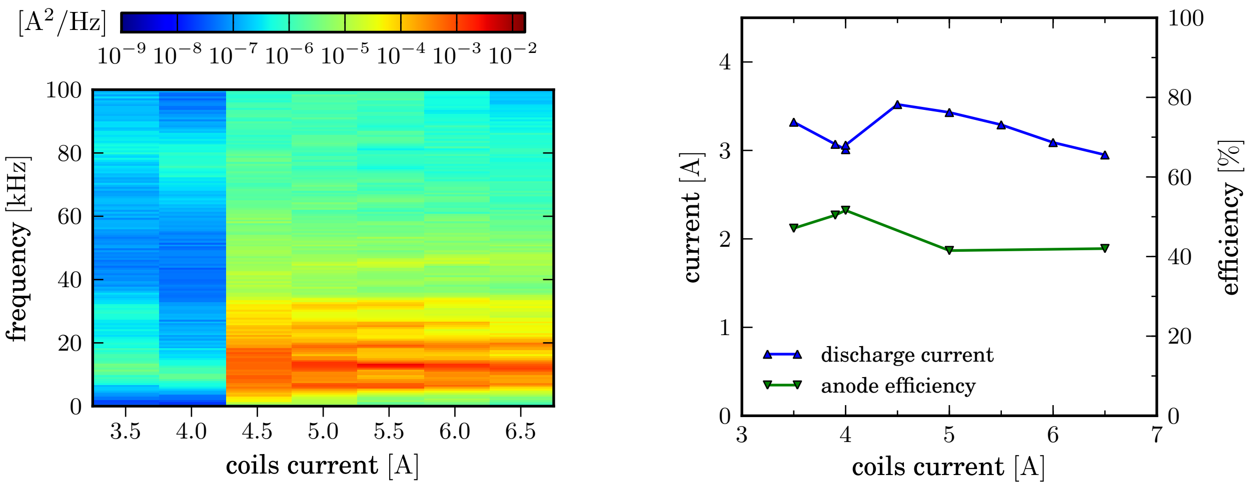

Figure 11: Power spectral density of the discharge current, average discharge current and anode efficiency as a function of the magnetic field with z, θ-partitioning, $\dot{m} = 3\,\mathrm{mg/s}$ and $U_d = 500\,\mathrm{V}$.

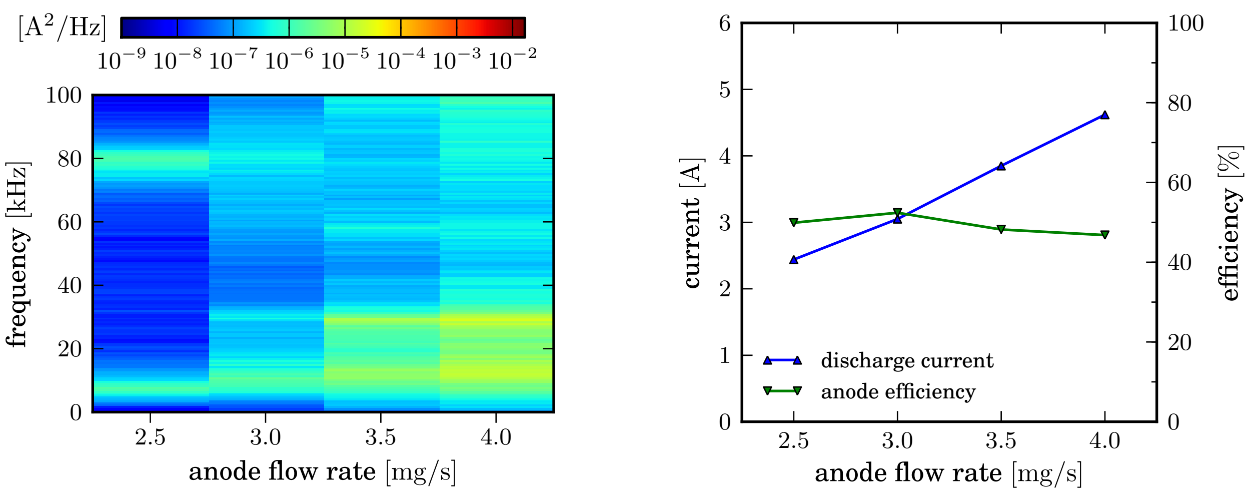

Figure 12: Power spectral density of the discharge current, average discharge current and anode efficiency as a function of the anode mass flow rate with z, θ-partitioning, coils current $4\,\mathrm{A}$ and $U_d = 500\,\mathrm{V}$.

VI. Conclusion

A theoretical estimate of the critical partition thickness for layered channels has been derived, based on the premise that in-wall conductivity should remain below the level of classical near-wall conductivity. The capability of a graphite-based partitioned channels to achieve highly efficient operation at high voltage has been demonstrated in two different experiments, using respectively axial and axial-azimuthal partitioning. Such composite material appears thus particularly promising for high-Isp operation, since on the one hand the efficiency of BN-based channels is usually strongly impacted by space charge saturation effects at high voltage, while on the other hand channel lifetime becomes critical due to the presence of energetic xenon ions. Further studies and investigations are necessary, however, to refine the mechanical design and assess the long-term behavior of such channel in terms of both efficiency and erosion.

Acknowledgments

This work has been performed with the support of the French Research Group "Propulsion par plasma dans l'espace" (GDR 3161 CNRS/CNES/SNECMA/Universités).

References

[1]Raitses, Y., Keidar, M., Staack, D., and Fisch, N. J., "Effects of Segmented Electrode in Hall Current Plasma Thrusters," *J. Appl. Phys.*, Vol. 92, 2002, pp. 4906.

[2]Gascon, N., Dudeck, M., and Barral, S., "Wall Material Effects in Stationary Plasma Thrusters. I. Parametric studies of an SPT-100," *Phys. Plasmas*, Vol. 10, 2003, pp. 4123.

[3]Raitses, Y., Staack, D., Dunaevsky, A., and Fisch, N. J., "Operation of a Segmented Hall Thruster with Low-Sputtering Carbon-Velvet Electrodes," *J. Appl. Phys.*, Vol. 99, 2006, pp. 036103.

[4]Diamant, K. D., Pollard, J. E., Cohen, R. B., Raitses, Y., and Fisch, N. J., "Segmented Electrode Hall Thruster," *J. Propul. Power*, Vol. 22, 2006, pp. 1396.

[5]Barral, S., Makowski, K., Peradzyński, Z., Gascon, N., and Dudeck, M., "Wall Material Effects in Stationary Plasma Thrusters. II. Near-Wall and In-Wall Conductivity," *Phys. Plasmas*, Vol. 10, 2003, pp. 4137.

[6]Rubin, B., Topper, J. L., and Yalin, A. P., "Total and Differential Sputter Yields of Boron Nitride Measured by Quartz Crystal Microbalance," *J. Phys. D: Appl. Phys.*, Vol. 42, 2009, pp. 205205.

[7]Garnier, Y., Viel, V., J.-F.Roussel, and Bernard, J., "Low-Energy Xenon Ion Sputtering of Ceramics Investigated for Stationary Plasma Thrusters," *J. Vac. Sci. Technol. A*, Vol. 17, 1999, pp. 3246.

[8]Kim, V., Kozlov, V., Semenov, A., and Shkarban, I., "Investigation of the Boron Nitride Based Ceramics Sputtering Yield under its Bombardment by Xe and Kr ions," *Proc. 27th International Electric Propulsion Conference*, No. 01-073, The Electric Rocket Propulsion Society, Worthington, OH, Pasadena, CA, 2001.

[9]Doerner, R. P., Whyte, D. G., and Goebel, D. M., "Sputtering Yield Measurements During Low Energy Xenon Plasma Bombardment," *J. Appl. Phys.*, Vol. 93, 2003, pp. 5816.

[10]Rosenberg, D. and Wehner, G. K., "Sputtering Yields for Low-Energy $He^{+}-$, $Kr^{+}-$ and $Xe^{+}-$ Ion Bombardment," *J. Appl. Phys.*, Vol. 33, 1962, pp. 1842.

[11]Tartz, M., Neumann, H., Leiter, H., and Esch, J., "Pyrolytic Graphite And Carbon-Carbon Sputter Behaviour Under Xenon Ion Incidence," *Proc. 29th International Electric Propulsion Conference*, No. 05-143, The Electric Rocket Propulsion Society, Worthington, OH, Princeton, NJ, 2005.

[12]Williams, J. D., Johnson, M. L., and Williams, D. D., "Differential Sputtering Behavior of Pyrolytic Graphite and Carbon-Carbon Composite Under Xenon Bombardment," *Proc. 40th AIAA Joint Propulsion Conference*, No. 2004-3788, American Institute of Aeronautics and Astronautics, Washington, D.C., Fort Lauderdale, FL, 2004.

[13]Meezan, N. B., Gascon, N., and Cappelli, M. A., "Linear Geometry Hall Thruster with Boron Nitride and Diamond Walls," *Proc. 27th International Electric Propulsion Conference*, No. 01-039, The Electric Rocket Propulsion Society, Worthington, OH, Pasadena, CA, 2001.

[14]Gascon, N., Crawford, W. S., Corey, R. L., and Capelli, M. A., "Coaxial Hall Thruster with Diamond Inner Channel Wall," *Proc. 42nd AIAA Joint Propulsion Conference*, No. 2006-4995, American Institute of Aeronautics and Astronautics, Washington, D.C., Sacramento, CA, 2006.

[15]Wu, J. and McLachlan, D. S., "Percolation Exponents and Tresholds Obtained from the Nearly Ideal Continuum Percolation System Graphite-Boron Nitride," *Phys. Rev. B*, Vol. 56, 1997, pp. 1236.

[16]Viel-Inguimbert, V., "Secondary Electron Emission of Ceramics used in the Channel of SPT," *Proc. 28th International Electric Propulsion Conference*, No. 03-258, The Electric Rocket Propulsion Society, Worthington, OH, Toulouse (France), 2003.

[17]Dunaevsky, A., Raitses, Y., and Fisch, N. J., "Secondary Electron Emission from Dielectric Materials of a Hall Thruster with Segmented Electrodes," *Phys. Plasmas*, Vol. 10, 2003, pp. 2574.

[18]Kirby, R. E., "Instrumental Effects in Secondary Electron Yield and Energy Distribution Measurements," *Proc. eCloud'04*, Napa Valley, CA, 2004.

[19]Pedgley, J. M., McCracken, G. M., Farhang, H., and Blott, B. H., "Measurements of Secondary Electron Emission for Fusion Related Materials," *J. Nucl. Mater.*, Vol. 196, 1992, pp. 1053.

[20]Zhakupov, A., Khartov, S., and Latyshev, L., "Hall Thruster with a Sectioned Conducting Channel," *Proc. 3rd International Spacecraft Propulsion Conference*, Cannes (France), 2000, p. 827.

[21]Fruchtman, A., Fisch, N. J., and Raitses, Y., "Control of the Electric-Field Profile in the Hall Thruster," *Phys. Plasmas*, Vol. 8, 2001, pp. 1048.

[22]Raitses, Y. and Fisch, N. J., "Parametric Investigations of a Nonconventional Hall Thruster," *Phys. Plasmas*, Vol. 8, 2001, pp. 2579.

[23]Raitses, Y., Staack, D., and Fisch, N. J., "Plasma Characterization of Hall Thruster with Active and Passive Segmented Electrodes," *Proc. 38th AIAA Joint Propulsion Conference*, No. 2002-3954, American Institute of Aeronautics and Astronautics, Washington, D.C., Indianapolis, 2002.

[24]Janes, G. S. and Lowder, R. S., "Anomalous Electron Diffusion and Ion Acceleration in a Low-Density Plasma," *Phys. Fluids*, Vol. 9, 1966, pp. 1115.

[25]Esipchuk, Y. B., Morozov, A. I., Tilinin, G. N., and Trofimov, A. V., "Plasma Oscillations in Closed-Drift Accelerators with an Extended Acceleration Zone," *Sov. Phys. Tech. Phys.*, Vol. 18, 1974, pp. 928.

[26]Choueiri, E. Y., "Plasma Oscillations in Hall Thrusters," *Phys. Plasmas*, Vol. 8, 2001, pp. 1411.